



# Polyimide Aerogel Fibers with Controllable Porous Microstructure for Super-Thermal Insulation Under Extreme Environments

Tiantian Xue<sup>1</sup> · Chenyu Zhu<sup>1</sup> · Xueling Feng<sup>1</sup> · Qamar Wali<sup>3</sup> · Wei Fan<sup>1</sup> · Tianxi Liu<sup>1,2</sup>

Received: 15 December 2021 / Accepted: 29 January 2022 / Published online: 5 April 2022  
© Donghua University, Shanghai, China 2022

## Abstract

Application of aerogel fibers in thermal insulating garments have sparked a substantial interest. However, achieving a high porosity and low thermal conductivity for aerogel fibers remain challenging, despite the innovative designs of porous structure. Herein, we fabricated lightweight and super-thermal insulating polyimide (PI) aerogel fibers via freeze-spinning by using polyvinyl alcohol (PVA) as a pore regulator. The high affinity of PVA with water enables it to accelerate the ice crystal nucleation, adjust pore formation, and construct a controllable porous structure of PI aerogel fiber. The as-fabricated PI aerogel fiber has a considerable reduced pore size, high porosity (95.6%), improved flexibility and mechanical strength, and can be woven into fabrics. The PI aerogel fabric exhibits low thermal conductivity and excellent thermal insulation in a wide range of temperature (from  $-196$  to  $300$  °C). Furthermore, the PI aerogel fabrics can be easily functionalized to expand their applications, such as in intelligent temperature regulation and photothermal conversion. These results demonstrate that the aerogel fibers/fabric are promising materials for next-generation textile materials for personal thermal management.

**Keywords** Polyimide · Aerogel fiber · Pore regulation · Thermal insulation · Thermal management

## Introduction

Due to increasing demands of saving energy and a wide range of personal thermoregulation requirements, thermoregulating textiles capable of offering thermal management technologies are preeminently important nowadays [1–3]. Particularly, personal thermal-insulating textiles that could keep the human body thermally comfortable are essential in extreme environments such as Polar Regions and

outer space [4–6]. However, traditional thermal insulation garments are mainly composed of cotton, down, and other filling materials, which are cumbersome and have poor thermal insulating effects [7, 8]. Therefore, developing novel, lightweight, and efficient personal thermal-insulating textiles is needed.

Low apparent density, ultrahigh porosity, and large surface area enable aerogels to block thermal conduction, convection, and radiation, making them an ideal thermal-insulating material [9–11]. Shaping the three-dimensional aerogels into one-dimensional aerogel fibers could apprehend the design and manufacturing of aerogel fabrics. Therefore, aerogel fibers and fabrics are expected to become the next generation lightweight, highly efficient thermal-insulating wearable garments. Recently, researchers have been working on aerogel fibers like inorganic silica aerogel fiber [12, 13] and organic aerogel fibers, such as Kevlar [14], silk [4, 15, 16], and cellulose aerogel fibers [17]. For example, Du et al. [12] prepared transparent silica aerogel fibers by reaction spinning, exhibiting a high specific surface area ( $890$  m<sup>2</sup> g<sup>-1</sup>), good thermal insulation, and broad temperature feasibility ( $-196$  to  $300$  °C), but their applications in wearable garments are largely limited due to low tensile strength ( $\sim 150$  kPa). Contrarily, the burgeoning

✉ Wei Fan  
weifan@dhu.edu.cn

✉ Tianxi Liu  
txliu@dhu.edu.cn

<sup>1</sup> State Key Laboratory for Modification of Chemical Fibers and Polymer Materials, College of Materials Science and Engineering, Donghua University, 2999 North Renmin Road, Shanghai 201620, People's Republic of China

<sup>2</sup> Key Laboratory of Synthetic and Biological Colloids, Ministry of Education, School of Chemical and Material Engineering, Jiangnan University, Wuxi 214122, People's Republic of China

<sup>3</sup> School of Applied Sciences and Humanities, National University of Technology, Islamabad 42000, Pakistan

organic aerogel fibers have higher tensile strength compared to inorganic silica aerogel fibers. For instance, Kevlar aerogel fibers were fabricated through wet spinning from Kevlar nanofibrous dispersion, which presented excellent thermal insulation ability, high tensile strength (3.3 MPa), and high specific surface area [14]. Nevertheless, wet spinning often requires the troublesome solvent exchange and time-consuming supercritical drying to obtain the final aerogel fibers [18]. To overcome this, Cui et al. [4] reported a freeze-spinning method to fabricate silk aerogel fibers with an axially aligned porous structure, exhibiting excellent thermal insulation property. This freeze-spinning method combines “directional freezing” with “solution spinning”, enabling large-scale and continuous fabrication of aerogel fibers with tunable porous structure, which makes it a potential strategy for preparing aerogel fibers and fabrics.

Polyimide (PI) fibers have attracted widespread attention due to their excellent tensile strength, high-temperature stability, and low-temperature flexibility [19, 20]. In our previous work, we used the freeze-spinning technique to prepare polyimide aerogel fibers having high tensile strength, excellent fire-retardanting ability, and good thermal-insulating performance [21]. However, the fabrics that are woven with the above-mentioned aerogel fibers still have higher thermal conductivity compared with inorganic silica aerogels. Therefore, the reduction of the thermal conductivity of the polyimide aerogel fibers/fabrics is crucial for their wider applications. Previous reports revealed that thermal transfer is closely related to the density, porosity, and pore size of the material [22]. Particularly, the pore size of aerogel fiber is a key factor affecting its thermal insulation behavior. Aerogels with smaller pore sizes can increase the number of solid-air interfaces, which results in multiple scattering at the interface and increases the path of solid thermal conduction that improves thermal insulation [23, 24]. Therefore, controllable construction of the pore size of aerogel fibers implicates the improved thermal insulating performance. Previous reports have shown that combining nanoparticles with a polymer solution or changing the freezing temperature could regulate the pore size of aerogels [25–28]. However, these methods require sophisticated equipment, and the agglomeration of nanoparticles hinders their applicability. Therefore, it is crucial to develop alternative strategies to regulate the pore size of aerogel fibers and improve relevant thermal insulation properties.

In this study, polyvinyl alcohol (PVA) was used as a pore regulator, to fabricate lightweight and super-thermal insulating PI aerogel fibers with controllable porous microstructure through freeze-spinning. PVA as an ice crystal nucleating agent can affect ice crystal growth and adjust pore size because of the abundant hydroxyl groups that exhibit high affinity with water molecules. The thermal conductivity of PI aerogel fabrics is optimized by

adjusting the porous structure via PVA, achieving a low thermal conductivity of  $28.7 \pm 2.0 \text{ mW m}^{-1} \text{ K}^{-1}$ . Moreover, the PI aerogel fabric is flexible in an ultra-low temperature environment ( $-196 \text{ }^\circ\text{C}$ ) and can work under high temperatures (up to  $300 \text{ }^\circ\text{C}$ ). In addition, the PI aerogel fabrics could also function as intelligent temperature regulation and photothermal conversion fabrics when being incorporated with polyethylene glycol (PEG) and carbon nanotubes (CNTs), respectively. Therefore, the as-prepared PI aerogel fabric is potent as a lightweight personal thermal management garment in an extreme environment.

## Experimental Section

### Materials

Biphenyl 3,3',4,4',-teracarboxylic dianhydride (BPDA, 99.0%), 4,4',-diaminodiphenyl ether (ODA, 98.0%), *N,N*-dimethylacetamide (DMAc, 99.0%), and triethylamine (TEA, > 99.5%) were all provided by Sinopharm Chemical Reagent Co, Ltd. Polyvinyl alcohol (PVA,  $M_w \approx 80,000\text{--}124,000$ ) was acquired from Aladdin Chemistry Co., Ltd, China. Poly (ethylene glycol) (PEG,  $M_w = 1000$ ) was supplied by Sinopharm Chemical Reagent Co. Multi-walled carbon nanotubes (CNT, length: > 10  $\mu\text{m}$ ) were purchased from Chengdu Organic Chemicals Co. Ltd.

### Preparation of Polyimide (PI-x) Aerogel Fiber

According to our previous work, water-soluble poly(amic acid) (PAA) salt was synthesized from BPDA and ODA [29]. The PAA/PVA spinning solution was prepared by mixing PAA and PVA in aqueous solution. The weight ratio of PAA to water was fixed to 5:100, and the weight ratio of PAA to PVA was set to 10:1, 10:2 and 10:3. The PAA/PVA solution was magnetically stirred for 24 h to become a transparent and viscous PAA/PVA spinning solution. The PI aerogel fibers were prepared by freeze-spinning, freeze-drying, and subsequent thermal imidization. The PAA/PVA spinning solution was squeezed out through a pump-controlled syringe, through a temperature-controlled copper ring to freeze the gel fibers gradually, and finally collected by a collecting rod. At the end, the collected fibers were freeze-dried, and then thermally imidized in a tube furnace at  $350 \text{ }^\circ\text{C}$  under an inert atmosphere to obtain PI aerogel fibers. The samples prepared with different mass ratios of PAA to PVA (10:1, 10:2 and 10:3) were designated as PI-10, PI-20 and PI-30, respectively.

## Preparation of Composite Fabrics with Phase-Change Material (PCM)

The PI-20 aerogel fabrics were soaked in the PEG1000 and placed in vacuum oven with 70 °C for 12 h, for PEG1000 infusion into the PI aerogel fibers. Afterwards, the excess PEG1000 was removed by filter papers to obtain the final PI/PCM composite fabrics.

## Preparation of Composite Fabrics for Photothermal Conversion

The PI-20 aerogel fibers were woven into a fabric (5 cm × 5 cm), and CNT in isopropanol suspension (2 mg mL<sup>-1</sup>) was sprayed on top of the PI-20 aerogel fabric surface repeatedly to ensure complete coverage and then dried under vacuum to obtain the PI/CNT composite fabrics.

## Characterization

The microstructure of the PI aerogel fiber was investigated by field-emission scanning electron microscopy (FESEM, JSM-7500F, JEOL, Japan) operating at 5 kV. Mechanical properties of PI aerogel fibers/fabrics were tested by an electronic universal testing machine (UTM2102, Suns Technology Stock Co., Ltd, China) with a sensor of 50 N. All thermal images were acquired via a thermal imager (TiS40, Fluke Co., Ltd, USA) at working distance of 20 cm. The thermal conductivity ( $\lambda$ ) of PI aerogel fabrics at different temperatures was measured with a hot disk thermal analyzer (Hot Disk TPS 2500S, Sweden). The thermogravimetric analysis (TGA) was performed by a thermogravimetric analyzer (F1 Libra, Netzsch Co., Ltd, German) with heating rate of 10 °C min<sup>-1</sup>. The phase change enthalpy was computed on a differential scanning calorimeter (DSC-822, Sweden) with heating rate of 10 °C min<sup>-1</sup>. The temperature–time curves were recorded by the thermal couple (175T2, testo Co., Ltd, China). The porosities of PI aerogel fiber were calculated using the following equation:

$$P = \left(1 - \frac{\rho_0}{\rho}\right) \times 100,$$

where  $P$  is the porosity,  $\rho_0$  is the apparent density, and  $\rho$  is the skeletal density, which is estimated from the density of polyimide (1.4 g cm<sup>-3</sup>).

## Results and Discussions

The fabrication process of PI aerogel fibers and fabrics is schematically illustrated in Fig. 1a, which involves freeze-spinning, freeze-drying, thermal imidization and weaving. The PAA/PVA spinning solution was first extruded through a syringe, before being passed through a temperature-controlled copper ring to gradually freeze the gel fibers. The frozen fibers were gathered on a collecting rod and then freeze-dried to remove ice crystals to achieve its porous structure. PAA was transformed into PI during the subsequent thermal imidization at 350 °C, while the PVA was removed because its decomposition began at ~280 °C (as shown by TGA curve in Fig. S1a), leaving the pure PI aerogel fiber [30–32]. Furthermore, FTIR spectra reveal the characteristic peaks at 3293 cm<sup>-1</sup> (–OH stretching vibration) and 2911 cm<sup>-1</sup> (–CH<sub>2</sub> asymmetric stretching vibration) for pure PVA (Fig. S1b) [33]. However, the characteristic peak of PVA in the FTIR of PI-20 disappeared, which also proved that PVA was completely removed after thermal imidization. The light weight PI aerogel fibers are highly porous (95.6% porosity) and have low density (0.06 g cm<sup>-3</sup>). Figure 1b depicts the image of the as-prepared PI aerogel fibers in a roll with approximately 400  $\mu$ m diameter and yellow color. Photograph of PI aerogel fiber knot displays the good flexibility and knittability of aerogel fibers (Fig. 1c). Moreover, the fiber shows high tensile strength and can withstand 200 g tensile load (Fig. 1d). Due to the outstanding flexibility and mechanical strength, the fiber could conveniently be woven into fabrics, providing the possibility for practical use in garments (Fig. 1e and Fig. S2).

The formation and growth of ice crystals in freeze-spinning process determines the micro-morphology of the aerogel fiber, similar to the ice template method [34]. The cross-sectional microstructure of PI aerogel fibers with different content of PVA in the spinning solution is revealed by SEM images in Fig. 2a–h. All the aerogel fibers exhibit a three-dimensional porous structure and different pore sizes that vary by changing the amount of PVA. The pure PI-0 aerogel fiber has large pore sizes (46.3 ± 12.6  $\mu$ m) with broad distribution (Fig. 2a, b and Fig. S3a). With the incorporation of PVA, the pore size of PI-10 aerogel fibers decreases to 41.5 ± 20  $\mu$ m (Fig. 2c, d and Fig. S3b). The PI-20 aerogel fiber with initial 20 wt% PVA exhibits the smallest pore size centered in 11.5 ± 4.5  $\mu$ m among those samples (Fig. 2e, f and Fig. S3c). However, further increase in the amount of PVA leads to the curved laminar porous structure as for PI-30 aerogel fiber, which is probably due to the fact that excess PVA promotes the nucleation and formation of ice crystals, forming lamellar ice crystals [35] (Fig. 2g, h and Fig. S3d). The surface of

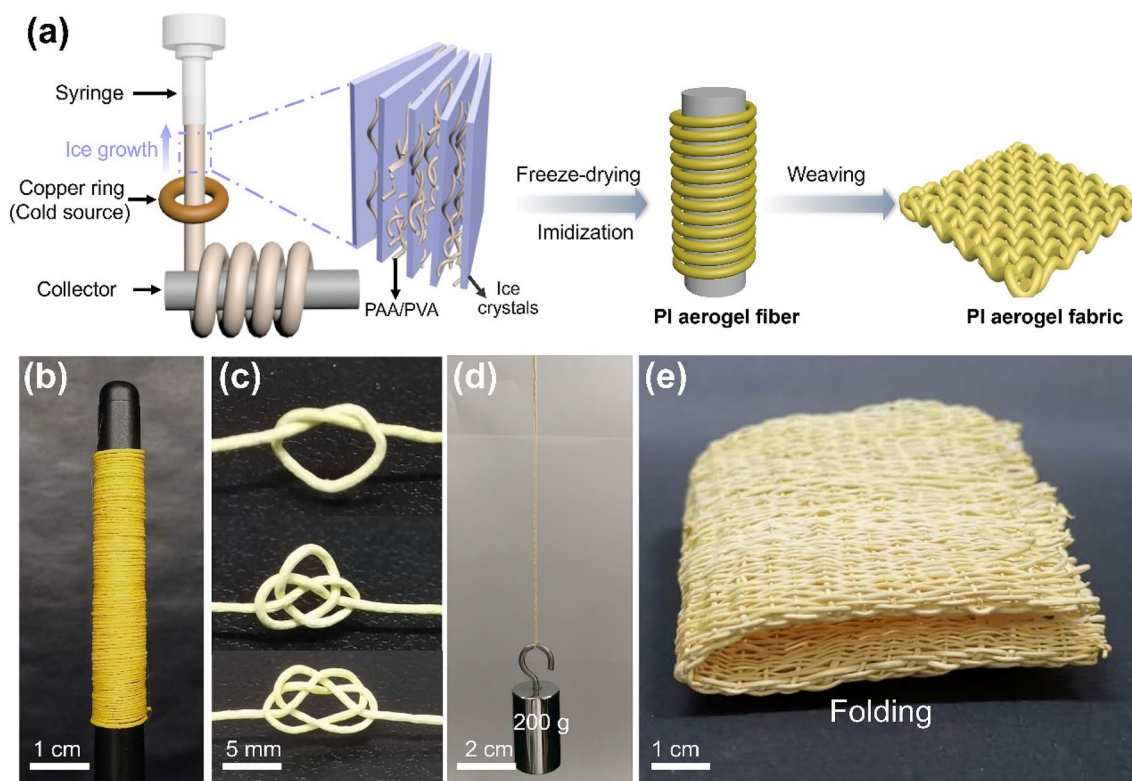


**Fig. 1** Fabrication of PI aerogel fibers and fabrics. **a** Schematic description of the fabrication process of PI aerogel fibers and fabrics. **b** Photograph of the PI aerogel fiber collected in a roll. **c** Pho-

tograph of PI aerogel fiber knot. **d** Photograph of a single PI aerogel fiber withstand weight of 200 g. **e** Photograph of a PI aerogel fabric (10 cm × 10 cm), reflecting its folding property

aerogel fibers is also uniformly porous structure, with the pore size decreasing as the PVA concentration increases (Fig. S4). The smaller pore size of PI-20 aerogel fibers is attributed to the strong interaction between PAA and PVA as well as PVA and water, as schematically illustrated in Fig. 2i. The interaction between the PAA chain and PVA can be deduced from the FTIR characterization (Fig. 2j). The strength of the hydroxyl absorption peak ( $3100\text{--}3650\text{ cm}^{-1}$ ) increases in PAA/PVA compared to PAA, whereas the wavenumber of the CO–NH bond decreases, showing a substantial interaction between PVA and water as well as PAA and PVA [36]. To further demonstrate the interaction between PAA and PVA, the rheological behaviors of the PAA and PAA/PVA solutions were carried out using a rotational rheometer as shown in Fig. S5. The viscosity of PAA/PVA increased significantly with increasing PVA content, demonstrating a strong interaction between PAA and PVA [37]. Due to the high affinity between PVA and water, it could accelerate the ice nucleation and increase the amount of ice crystals, resulting in smaller ice crystals and thus smaller pore size [35, 38]. This smaller pore size could significantly improve the thermal insulation of aerogel fibers.

The PI aerogel fibers, with up to 95.6% porosity, have a tremendous potential in the field of thermal insulating garments. PI aerogel fibers with diverse porous structures were placed on the same hot stage to compare their thermal insulating properties. Infrared images were captured at various temperatures ranging from  $-30$  to  $300\text{ }^{\circ}\text{C}$ , with three representative infrared images displayed in Fig. 3a, showing its advantages over a wide temperature range. The temperature difference ( $|\Delta T|$ ) between the PI aerogel fiber surface and the thermal platform is estimated and summarized in Fig. 3b via infrared images. With the decrease of pore size, the  $|\Delta T|$  increases, which indicates that smaller pores promote thermal insulation (Fig. 3c). However, the PI-30 aerogel fibers have higher  $|\Delta T|$  because the curved laminar porous structure can reduce the thermal conduction, at the same time it can form multiple thermal reflection interfaces. Figure 3d schematically illustrates the heat transfer through the aerogel fiber. Typically, thermal conductivity of aerogel fiber ( $\lambda_{\text{fiber}}$ ) is the sum of the thermal convection ( $\lambda_{\text{conv}}$ ), thermal conduction ( $\lambda_{\text{cond}}$ ), and thermal radiation ( $\lambda_{\text{rad}}$ ) [4]. The thermal convection ( $\lambda_{\text{conv}}$ ) of aerogel fiber is extremely limited because airflow is suppressed in micro-sized pores. The thermal radiation ( $\lambda_{\text{rad}}$ ) is negligible owing

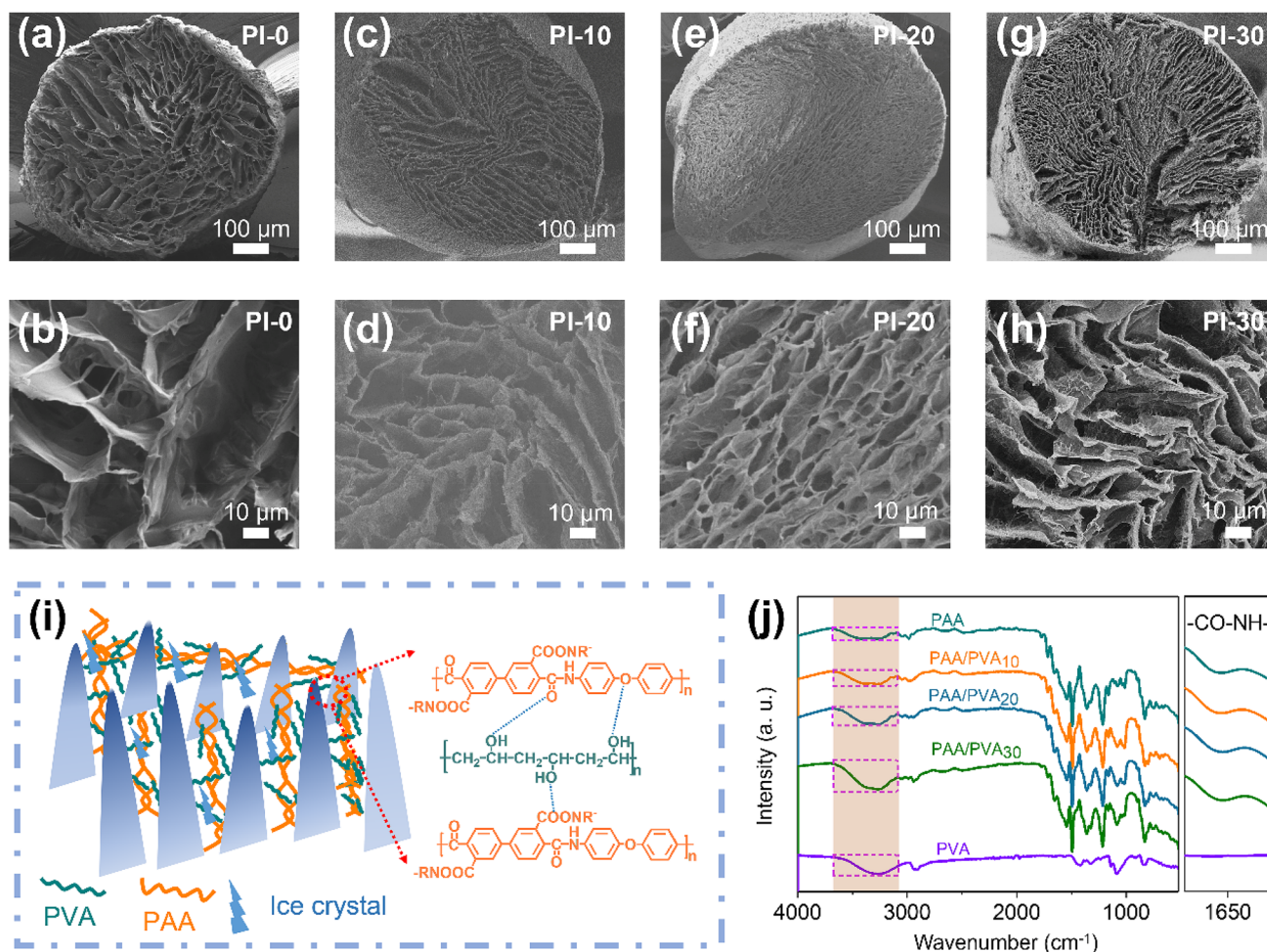


**Fig. 2** Morphological and chemical structural characterization of PI aerogel fibers. **a–h** SEM images of PI aerogel fibers with different initial content of PVA. **a, b** PI-0; **c, d** PI-10; **e, f** PI-20 and **g, h** PI-30. **i**

Schematic illustration for porous structure of aerogel fiber and interaction between PAA and PVA chains. **j** FTIR spectra of the PAA/PVA aerogel fibers with different contents of PVA

to the relatively low environment temperature [39]. The heat exchange via thermal conduction ( $\lambda_{\text{cond.}}$ ) is determined by solid conduction ( $\lambda_s$ ) and gas conduction ( $\lambda_g$ ), and strongly depends on the pore size. Reduction in the pore size can extend the path of solid conduction and reduce the movement of gas molecules. Furthermore, smaller pore size contributes to numerous solid-air interfaces that lead to multiple scattering at interfaces, resulting in reduced thermal conduction ( $\lambda_{\text{cond.}}$ ) of aerogel fibers. Therefore, pore size reduction can enhance the thermal insulation performance of the aerogel fiber. Moreover, mechanical properties are crucial for knittability and wearability of the aerogel fibers. Typical stress–strain curves for single PI aerogel fibers are shown in Fig. 3e. As the pore size decreases from  $46.3 \pm 12.6 \mu\text{m}$  to  $11.5 \pm 4.5 \mu\text{m}$ , the tensile strength raises from  $2.1 \pm 0.5$  to  $5.2 \pm 0.3$  MPa. At the same time, the modulus of PI-20 aerogel fiber is increased to  $35.2 \pm 4.0$  MPa (Fig. 3f). These results demonstrate that reducing the pore size dramatically

augments the thermal insulation and mechanical properties of aerogel fibers.

We further demonstrated the mechanical and thermal insulating performances of the PI aerogel fabric woven by PI-20 aerogel fibers. The PI aerogel fabric (weight 400 mg, size  $100 \text{ mm} \times 15 \text{ mm} \times 2 \text{ mm}$ ) could bear a load of more than 1250 times its own weight without damage, as presented in Fig. 4a. Typical stress–strain curves for PI aerogel fabrics demonstrate a tensile strength of  $2.2 \pm 0.2$  MPa, as shown in Fig. S6. Furthermore, the PI aerogel fabric can be folded and released repeatedly in liquid nitrogen without any damage (Fig. 4b) and Video S1, illustrating its outstanding flexibility in the low temperature environment. For thermal insulation applications, the PI aerogel fabric is placed on a thermal platform and compared to commercial cotton and polyester fabric (Fig. 4c). At a stage temperature of  $300 \text{ }^\circ\text{C}$ , the PI aerogel fabric was thermally stable with decomposition temperature of up to  $500 \text{ }^\circ\text{C}$  (TGA curves shown in Fig.

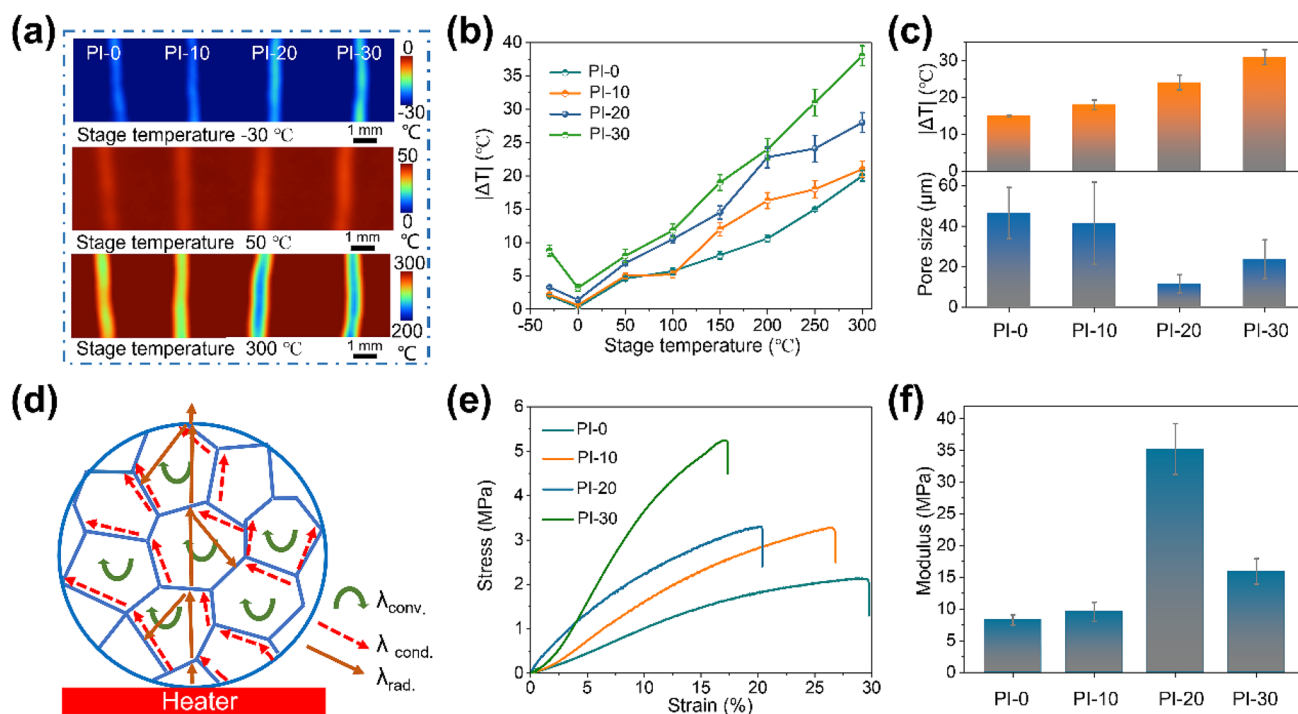


**Fig. 3** Mechanical and thermal insulating property of PI aerogel fibers. **a** Infrared images of PI aerogel fibers with different porous structures on thermal platform with different temperatures. **b** Temperature difference ( $\Delta T$ ) between the PI aerogel fiber surface and the thermal platform, at various platform temperatures ranging from  $-30$  to

$300$  °C. **c** Temperature difference ( $\Delta T$ ) is correlated with the pore size of corresponding PI aerogel fibers. **d** Schematic diagram of heat transfer of the aerogel fiber. **e** Tensile stress versus strain curves and **f** modulus of PI aerogel fibers

S7) and its average surface temperature was  $220$  °C. Contrarily, the cotton pyrolyzed and polyester melted on the stage after 3 min, as can be inferred from the corresponding TGA and DSC curves (Fig. S8). As obvious by the temperature difference ( $\Delta T$ ) in Fig. 4d, The PI aerogel fabric showed a higher  $|\Delta T|$  than cotton and polyester from  $-30$  to  $300$  °C, indicating its excellent thermal insulation performance over a wide temperature range (Fig. 4d). The corresponding thermal conductivity of the PI aerogel fabric was only  $28.7 \pm 2.0$  mW  $m^{-1} K^{-1}$  at  $25$  °C and slightly increased as the temperature raised to  $300$  °C (Fig. 4e). Besides, the thermal insulating property of the PI aerogel fabric exhibited long-time stability under high and low temperature environment, without temperament fluctuation (Fig. S9). As an example, a hand could be placed on ice or a hot stage with  $100$  °C with a piece of PI aerogel fabric (Fig. S10), demonstrating its great potential as thermal protective clothing.

On the same wrists, PI aerogel fabric (thickness: 4 mm) is compared with cotton fabric (thickness: 4 mm) to further demonstrate the wearability and thermal insulation of aerogel fabrics. The infrared thermal imager did not detect the wrist covered by PI aerogel fabric, proving its infrared thermal stealth function, which is expected to be applied to the infrared thermal stealth garments for soldiers [40]. The temperature difference ( $\Delta T$ ) between the surface of

PI aerogel fabric and the skin is as high as  $10.8$  °C that is twice that of cotton fabric, indicating the excellent thermal insulating properties as clothing for practical use (Fig. 4g).

In addition to preventing the heat transfer, the PI aerogel fabrics must be breathable in order to improve human comfort (Fig. S11a). We compared the breathability of PI aerogel fabrics with commercial cotton fabrics. Hot steam can pass through the PI aerogel fabrics smoothly and the amount of water vapor in the upper part of the beaker is almost equivalent to that of cotton (Fig. S11b). As for the water vapor transmission rate, the air permeability of the PI aerogel fabrics is comparable to that of cotton fabrics (Fig. S11c). At the same time, the hydrophobicity of the PI aerogel fabrics (water contact angle of  $101.7^\circ$ ) further improves the wearing comfort (Fig. S11d). Therefore, the PI aerogel fabrics are hydrophobic and breathable, which can meet the requirements for human wearing.

The PI aerogel fabrics can be easily functionalized to broaden the horizon of their applications, such as intelligent temperature regulating and photothermal conversion. The PI aerogel fabrics can be combined with PCM such as PEG for temperature regulation in the microclimate near the human skin, providing comfortable temperature environment for the human body [41]. Due to its high porosity and strong capillary force, the PI aerogel fiber can load high content of PEG

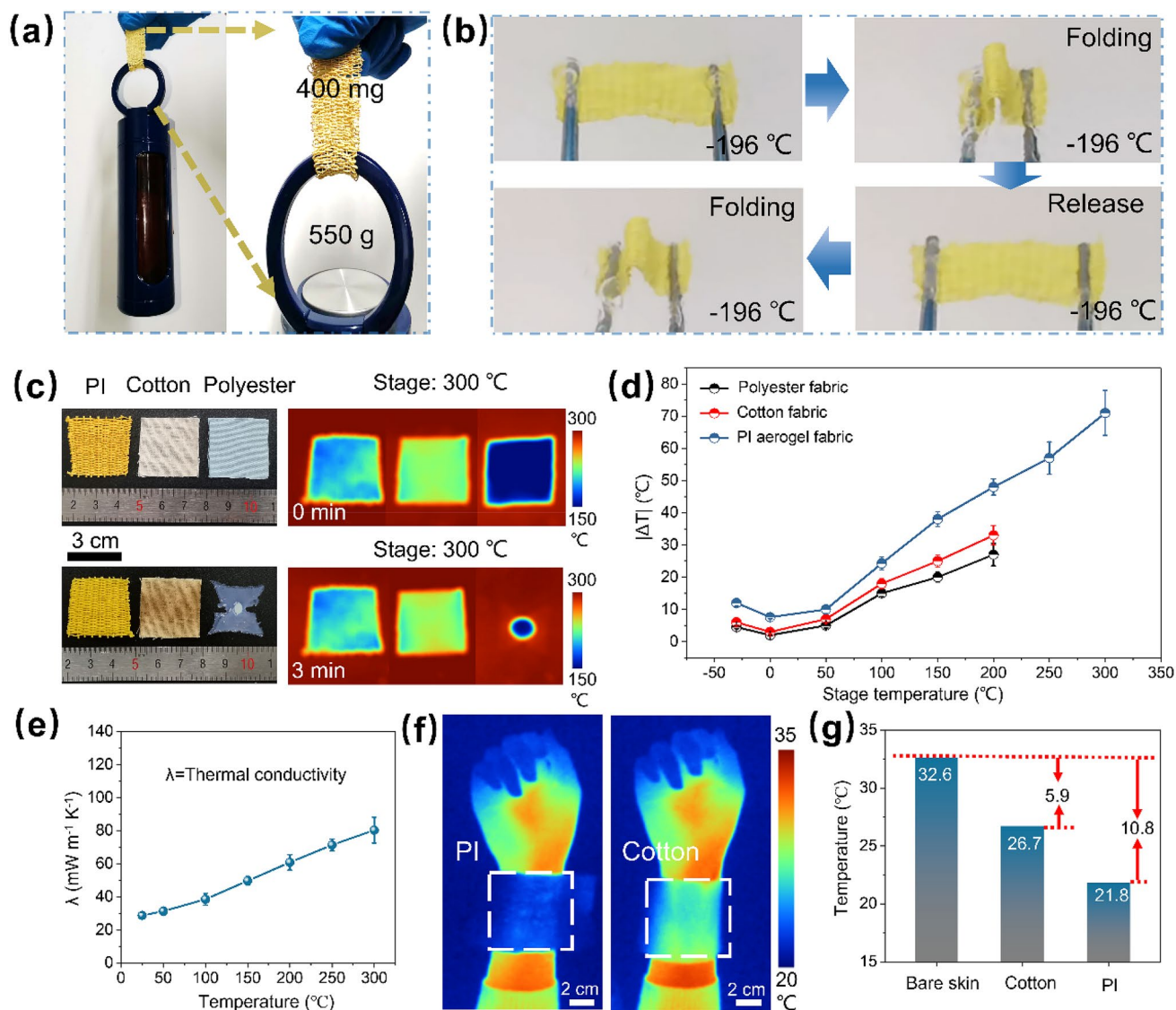


**Fig. 4** Mechanical and thermal insulating performances of the PI aerogel fabric. **a** Photograph shows the PI aerogel fabric withstanding a tensile load of 500 g. **b** Photograph of the PI aerogel fabric immersed into liquid nitrogen with subsequent folding and release. **c** Photograph and infrared images of the PI aerogel, cotton and polyester fabrics placed on the 300 °C thermal platform for 3 min. **d** Tem-

perature difference ( $\Delta T$ ) between the fabric surface and the thermal platform are correlated with different fabrics. **e** Thermal conductivity ( $\lambda$ ) of the PI aerogel fabric at diverse environmental temperatures. **f** spectra images of PI aerogel fabric and cotton fabric covered on skin, and **g** corresponding surface temperature of bare skin, cotton and PI aerogel fabric

without leakage during use. The TGA curves display that the loading content of PEG is 91.3% (Fig. S12a). At the same time, the DSC curve of the PI/PCM composite fabric is shown in Fig. S12b, demonstrating the high energy storage performance with phase change enthalpy of  $161.2 \text{ J g}^{-1}$ . The temperature regulating ability of PI/PCM composite fabric was detected by simulating the change of external temperature with the hot stage, and the device is schematically illustrated in Fig. 5a. The surface temperature change of PI/PCM composite fabric was detected by infrared thermal camera in Fig. 5b. Upon heating for 5 min, the surface temperature of the PI/PCM

composite fabric was only  $41.0 \text{ }^\circ\text{C}$ , while that of PI aerogel fabric rapidly increased to  $48.0 \text{ }^\circ\text{C}$ . After cooling for 5 min, the surface temperature of the PI/PCM composite fabric remained  $35.4 \text{ }^\circ\text{C}$ , while that of PI aerogel fabric rapidly decreased to  $27.0 \text{ }^\circ\text{C}$  (Fig. S13). This is mainly due to the phase change of PEG, which can delay the temperature change during the external temperature variation [42]. However, the final surface temperature of PI/PCM composite fabric ( $55.6 \text{ }^\circ\text{C}$  at 15 min) is higher than that of PI aerogel fabric ( $52.6 \text{ }^\circ\text{C}$  at 15 min), due to the low thermal conductivity of PI aerogel fabric. To further suppress the heat loss, a double-layer fabric is proposed

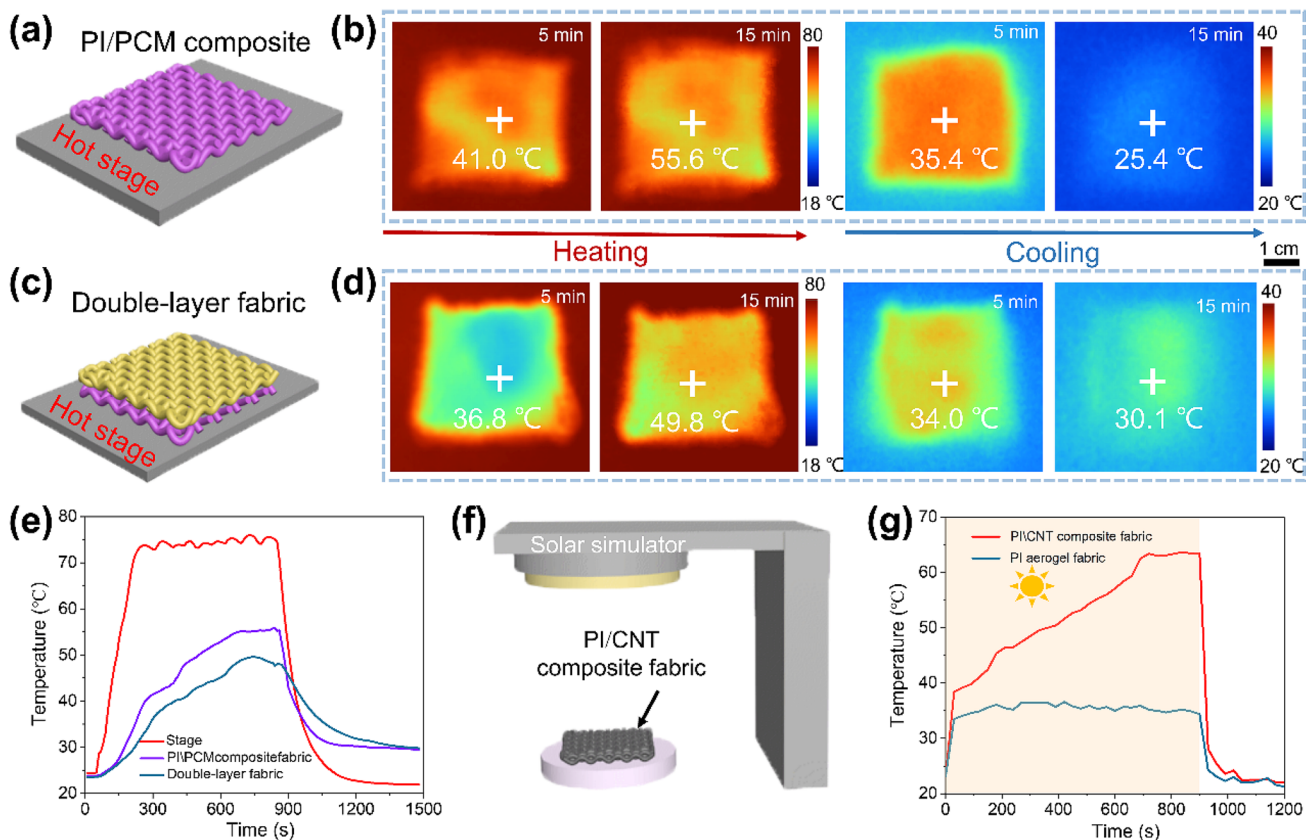


**Fig. 5** Multifunctionality of the composite fabric. **a** Schematic illustration of the device for testing the thermal regulation of the PI/PCM composite fabric. **b** Infrared images showing the PI/PCM composite fabric over heating–cooling cycle (25–80 °C). **c** Schematic illustration of the device for the double-layer fabric. **d** Infrared images showing the double-layer fabric over a heating–cooling cycle (25–80 °C).

by combing PI aerogel fabric and PI/PCM composite fabric to achieve the bifunctionality of temperature regulation and thermal insulation, as illustrated in Fig. 5c. The surface temperature change of double-layer fabric was detected by infrared thermal imager in Fig. 5d and plotted in Fig. 5e. The infrared images show that the upper surface temperature of the double-layer fabric is lower than that of the one-layer PI/PCM fabric during the heating process, due to the thermal insulating ability of the PI aerogel fabric. During the cooling process, the temperature of double-layered fabric decreased slowly, which can be maintained at about 30 °C even if the external temperature is 20 °C. This double-layer fabric could effectively suppress heat loss and regulate heat during the external temperature changes, making it promising candidate for highly efficient personal thermal management clothes. In addition, composite fabric for photothermal conversion was prepared by spraying CNTs on the surface of PI aerogel fabric for human heating. The experimental device for photothermal conversion of the composite fabric was illustrated in Fig. 5f. The PI/CNT composite fabric and PI aerogel fabric were exposed to 100

mW cm<sup>-2</sup> light irradiation for 15 min and then the light was removed, and the temperature was detected by infrared thermal imager as plotted in Fig. 5g. As observed, the temperature rising speed of PI/CNT composite fabric is significantly higher than that of PI aerogel fabric under light irradiation, proving its good photothermal conversion ability that is attributed to the better light-absorbing ability of CNT [43, 44]. In addition, CNTs are evenly distributed and adhered firmly on the PI aerogel fabric, which can be washed in water (Fig. S14), making it practically applicable. Therefore, the PI aerogel based composite fabrics with multi-functionality are potential smart material for intelligent thermal management.

### Conclusions

In conclusion, using freeze-spinning, PI-20 aerogel fibers with high porosity (95.6%), good mechanical, and thermal insulating properties have been fabricated from PAA/PVA solution. The pore size of PI aerogel fiber can be reduced

from  $46.3 \pm 12.6$  to  $11.5 \pm 4.5$   $\mu\text{m}$  using PVA as an ice crystal nucleating agent. The PI aerogel fabric woven from the PI aerogel fibers exhibits low thermal conductivity and excellent thermal insulation at extremely low temperature ( $-196$  °C), such as liquid nitrogen, and high temperature ( $300$  °C); owing to its small pore size and high porosity. Furthermore, the PI aerogel fabrics can be easily functionalized with PCM or CNT, to prepare intelligent temperature regulating or photothermal conversion fabric, further expanding their potential applications in personal thermal management. In addition, our strategy of using PVA as a pore regulator is simple and efficient, providing alternative method for preparing porous materials.

**Supplementary Information** The online version contains supplementary material available at <https://doi.org/10.1007/s42765-022-00145-8>.

**Acknowledgements** This work was supported by the National Natural Science Foundation of China (52073053), Shanghai Rising-Star Program (21QA1400300), Innovation Program of Shanghai Municipal Education Commission (2021-01-07-00-03-E00108), Science and Technology Commission of Shanghai Municipality (20520741100), and China Postdoctoral Science Foundation (2021M690596).

## Declarations

**Conflict of interest** The authors declare no competing financial interest.

## References

- Peng YC, Cui Y. Advanced textiles for personal thermal management and energy. *Joule* **2020**;4:724–42.
- Hu R, Liu YD, Shin SM, Huang SY, Ren XC, Shu WC, Cheng JJ, Tao GM, Xu WL, Chen RK, Luo XB. Emerging materials and strategies for personal thermal management. *Adv Energy Mater* **2020**;10:1903921.
- Ruan KP, Shi XT, Guo YQ, Gu JW. Interfacial thermal resistance in thermally conductive polymer composites: a review. *Compos Commun* **2020**;22:100518.
- Cui Y, Gong HX, Wang YJ, Li DW, Bai H. A thermally insulating textile inspired by polar bear hair. *Adv Mater* **2018**;30:1706807.
- Wang H, Cao M, Zhao HB, Liu JX, Geng CZ, Wang YZ. Double-cross-linked aerogels towards ultrahigh mechanical properties and thermal insulation at extreme environment. *Chem Eng J* **2020**;399:125698.
- Ma ZH, Zhao DL, She C, Yang Y, Yang RG. Personal thermal management techniques for thermal comfort and building energy saving. *Mater Today Phys.* **2021**;20:100465.
- Tang Y, Yu H, Wang Z, Luo MH, Zhang KG, Jiao Y, Li CE. Typical winter clothing characteristics and thermal insulation of ensembles for older people in china. *Build Environ* **2020**;182:107127.
- Pakdel E, Naebe M, Kashi S, Cai ZX, Xie WJ, Yuen ACY, Montazer M, Sun L, Wang XG. Functional cotton fabric using hollow glass microspheres: Focus on thermal insulation, flame retardancy, UV-protection and acoustic performance. *Prog Org Coat* **2020**;141:105553.
- Huang T, Zhu Y, Zhu J, Yu H, Zhang QH, Zhu MF. Self-reinforcement of light, temperature-resistant silica nanofibrous aerogels with tunable mechanical properties. *Adv Fiber Mater* **2020**;2:338–47.
- Zhang XX, Wang F, Dou LY, Cheng XT, Si Y, Yu JY, Ding B. Ultrastrong, superelastic, and lamellar multiarch structured  $\text{ZrO}_2\text{-Al}_2\text{O}_3$  nanofibrous aerogels with high-temperature resistance over  $1300$  °C. *ACS Nano* **2020**;14:15616–25.
- Jiang SH, Cheong JY, Nam JS, Kim ID, Agarwal S, Greiner A. High-density fibrous polyimide sponges with superior mechanical and thermal properties. *ACS Appl Mater Interfaces* **2020**;12:19006–14.
- Du Y, Zhang XH, Wang J, Liu ZW, Zhang K, Ji XF, You YZ, Zhang XT. Reaction-spun transparent silica aerogel fibers. *ACS Nano* **2020**;14:11919–28.
- Meng S, Yu SL, Tang FY, Hu XN, Lu J, Fei X, Zhu MF. Fiber engineering of silica-based aerogels with surface specificity and regenerability for continuous removal of dye pollutants from wastewaters. *Microporous Mesoporous Mater* **2021**;314:110874.
- Liu ZW, Lyu J, Fang D, Zhang XT. Nanofibrous Kevlar aerogel threads for thermal insulation in harsh environments. *ACS Nano* **2019**;13:5703–11.
- Wu JW, Hu R, Zeng SN, Xi W, Huang SY, Deng JH, Tao GM. Flexible and robust biomaterial microstructured colored textiles for personal thermoregulation. *ACS Appl Mater Interfaces* **2020**;12:19015–22.
- Shao ZY, Wang YJ, Bai H. A superhydrophobic textile inspired by polar bear hair for both in air and underwater thermal insulation. *Chem Eng J* **2020**;397:125441.
- Zhou J, Hsieh YL. Nanocellulose aerogel-based porous coaxial fibers for thermal insulation. *Nano Energy* **2020**;68:104305.
- Li MM, Gan F, Dong J, Fang YT, Zhao X, Zhang QH. Facile preparation of continuous and porous polyimide aerogel fibers for multifunctional applications. *ACS Appl Mater Interfaces* **2021**;13:10416–27.
- Zhang MY, Niu HQ, Wu DZ. Polyimide fibers with high strength and high modulus: preparation, structures, properties, and applications. *Macromol Rapid Commun* **2018**;39:1800141.
- Dong J, Yang CR, Cheng Y, Wu TT, Zhao X, Zhang QH. Facile method for fabricating low dielectric constant polyimide fibers with hyperbranched polysiloxane. *J Mater Chem C* **2017**;5:2818–25.
- Wang YJ, Cui Y, Shao ZY, Gao WW, Fan W, Liu TX, Bai H. Multifunctional polyimide aerogel textile inspired by polar bear hair for thermoregulation in extreme environments. *Chem Eng J* **2020**;390:124623.
- Zhang JY, Cheng YH, Tebyetekerwa M, Meng S, Zhu MF, Lu YF. “Stiff-Soft” binary synergistic aerogels with superflexibility and high thermal insulation performance. *Adv Funct Mater* **2019**;29:1806407.
- Zhan HJ, Wu KJ, Hu YL, Liu JW, Li H, Guo X, Xu J, Yang Y, Yu ZL, Gao HL, Luo XS, Chen JF, Ni Y, Yu SH. Biomimetic carbon tube aerogel enables super-elasticity and thermal insulation. *Chem* **2019**;5:1871–82.
- Fan W, Zhang X, Zhang Y, Zhang YF, Liu TX. Lightweight, strong, and super-thermal insulating polyimide composite aerogels under high temperature. *Compos Sci Technol* **2019**;173:47–52.
- Zhu XY, Yang C, Wu PW, Ma ZQ, Shang YY, Bai GZ, Liu XY, Chang G, Li N, Dai JJ, Wang XT, Zhang HL. Precise control of versatile microstructure and properties of graphene aerogel via freezing manipulation. *Nanoscale* **2020**;12:4882–94.
- Tian J, Yang Y, Xue TT, Chao GJ, Fan W, Liu TX. Highly flexible and compressible polyimide/silica aerogels with integrated double network for thermal insulation and fire-retardancy. *J Mater Sci Technol* **2022**;105:194–202.

27. Jiang QY, Liao X, Yang JM, Wang G, Chen J, Tian CX, Li GX. A two-step process for the preparation of thermoplastic polyurethane/graphene aerogel composite foams with multi-stage networks for electromagnetic shielding. *Compos Commun* **2020**;21:100416.
28. Yao KQ, Song CH, Fang H, Wang F, Chen L, Jiang SH, Zha GJ, Hou HQ. Freezing-extraction/vacuum-drying method for robust and fatigue-resistant polyimide fibrous aerogels and their composites with enhanced fire retardancy. *Engineering* **2021**. <https://doi.org/10.1016/j.eng.2021.08.024>.
29. Fan W, Zuo LZ, Zhang YF, Chen Y, Liu TX. Mechanically strong polyimide/carbon nanotube composite aerogels with controllable porous structure. *Compos Sci Technol* **2018**;156:186–91.
30. Zhang QR, Wang XY, Tao XJ, Li ZW, Li XH, Zhang ZJ. Polyvinyl alcohol composite aerogel with remarkable flame retardancy, chemical durability and self-cleaning property. *Compos Commun* **2019**;15:96–102.
31. Kang AH, Shang K, Ye DD, Wang YT, Wang H, Zhu ZM, Liao W, Xu SM, Wang YZ, Schiraldi DA. Rejuvenated fly ash in poly(vinyl alcohol)-based composite aerogels with high fire safety and smoke suppression. *Chem Eng J* **2017**;327:992–9.
32. Zhang XH, Ni XX, Li CX, You B, Sun G. Co-gel strategy for preparing hierarchically porous silica/polyimide nanocomposite aerogel with thermal insulation and flame retardancy. *J Mater Chem A* **2020**;8:9701–12.
33. Wang YT, Zhao HB, Degracia K, Han LX, Sun H, Sun M, Wang YZ, Schiraldi DA. Green approach to improving the strength and flame retardancy of poly(vinyl alcohol)/clay aerogels: Incorporating biobased gelatin. *ACS Appl Mater Interfaces* **2017**;9:42258–65.
34. Yang C, Zhu XY, Wang XT, Wang JS, Huang HB. Phase-field model of graphene aerogel formation by ice template method. *Appl Phys Lett* **2019**;115:111901.
35. Zhu ZC, Xiang JF, Wang JJ, Qiu D. Effect of polyvinyl alcohol on ice formation in the presence of a liquid/solid interface. *Langmuir* **2017**;33:191–6.
36. Li L, Zhang Y, Lu HY, Wang YF, Xu JS, Zhu JX, Zhang C, Liu TX. Cryopolymerization enables anisotropic polyaniline hybrid hydrogels with superelasticity and highly deformation-tolerant electrochemical energy storage. *Nat Commun* **2020**;11:62.
37. Xue TT, Fan W, Zhang X, Zhao XY, Yang F, Liu TX. Layered double hydroxide/graphene oxide synergistically enhanced polyimide aerogels for thermal insulation and fire-retardancy. *Compos B Eng* **2021**;219:108963.
38. Jin SL, Liu J, Lv JY, Wu SW, Wang JJ. Interfacial materials for anti-icing: Beyond superhydrophobic surfaces. *Chem Asian J* **2018**;13:1406–14.
39. Apostolopoulou-Kalkavoura V, Munier P, Bergström L. Thermally insulating nanocellulose-based materials. *Adv Mater* **2021**;33:2001839.
40. Lyu J, Liu ZW, Wu XH, Li GY, Fang D, Zhang XT. Nanofibrous Kevlar aerogel films and their phase-change composites for highly efficient infrared stealth. *ACS Nano* **2019**;13:2236–45.
41. Liu D, Lei C, Wu K, Fu Q. A multidirectionally thermoconductive phase change material enables high and durable electricity via real-environment solar-thermal-electric conversion. *ACS Nano* **2020**;14:15738–47.
42. Huang JW, Yu HY, Abdalkarim SYH, Marek J, Militky J, Li YZ, Yao JM. Electrospun polyethylene glycol/polyvinyl alcohol composite nanofibrous membranes as shape-stabilized solid-solid phase change materials. *Adv Fiber Mater* **2020**;2:167–77.
43. Liu H, Feng YY, Feng W. Alkyl-grafted azobenzene molecules for photo-induced heat storage and release via integration function of phase change and photoisomerization. *Compos Commun* **2020**;21:100402.
44. Li QT, Jiang MJ, Wu G, Chen L, Chen SC, Cao YX, Wang YZ. Photothermal conversion triggered precisely targeted healing of epoxy resin based on thermoreversible Diels–Alder network and amino-functionalized carbon nanotubes. *ACS Appl Mater Interfaces* **2017**;9:20797–807.

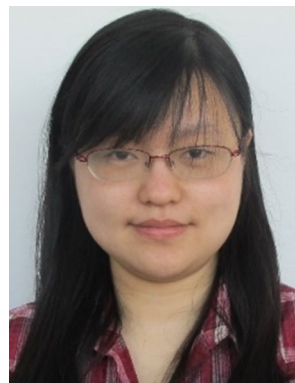
**Publisher's Note** Springer Nature remains neutral with regard to jurisdictional claims in published maps and institutional affiliations.



**Tiantian Xue** is a Ph.D. candidate in College of Materials Science and Engineering, Donghua University. She joined Prof. Tianxi Liu's group in 2018 and her research interest focuses on the polyimide aerogels for personal thermal management.



**Chenyu Zhu** is a postgraduate student in College of Materials Science and Engineering, Donghua University. He joined Prof. Tianxi Liu's group in 2020 and his research interest focuses on the polyimide aerogel fibers for thermal protection.



**Xueling Feng** is a professor of Donghua University, China. She received her B.S. and M.S. in Tsinghua University and obtained her Ph.D. degree from University of Twente, the Netherlands, in 2015. Prior to joining Donghua, she worked as a Research Fellow at Center of Biomimetic Sensor Science in Nanyang Technological University, Singapore. Her research interests are focused on the fabrication and applications of smart polymer and smart gel system for sensing and energy

harvesting.



**Qamar Wali** received his master's degree in Physics from University of Peshawar, Pakistan in 2009. He was awarded Ph.D. in Advanced Materials from Universiti Malaysia Pahang in 2016, Malaysia with distinction. Currently, he has been working as an Assistant Professor at National University of Technology (NUTECH) Islamabad, Pakistan since 2018. His current research is on selective contacts and the stability of perovskite solar cells.



**Tianxi Liu** is a Professor of the College of Materials Science and Engineering, Donghua University. He received his Ph.D. degree from Changchun Institute of Applied Chemistry, Chinese Academy of Sciences in 1998. His research interests include polymer nanocomposites, new energy materials and devices, hybrid materials, nanofibers and their composite materials.



**Wei Fan** is an Associate Professor of the College of Materials Science and Engineering, Donghua University. She received her Ph.D. degree in macromolecular chemistry and physics from Fudan University in 2015. Her research interests include aerogel composites and functional polymer nanocomposites.